Science of the Total Environment 650 (2019) 1980–1987

Contents lists available at ScienceDirect

Science of the Total Environment

journal homepage: www.elsevier.com/locate/scitotenv

Formation of Zn-Al layered double hydroxides (LDH) during the interaction of ZnO nanoparticles (NPs) with γ-Al_2O_3

Biao Wan [a], Yupeng Yan [a], Rixiang Huang [b], Dalton Belchior Abdala [c], Fan Liu [a], Yuanzhi Tang [b], Wenfeng Tan [a], Xionghan Feng [a,*]

[a] Key Laboratory of Arable Land Conservation (Middle and Lower Reaches of Yangtze River), Ministry of Agriculture, College of Resources and Environment, Huazhong Agricultural University, Wuhan 430070, China
[b] School of Earth and Atmospheric Sciences, Georgia Institute of Technology, 311 Ferst Dr, Atlanta, GA 30324-0340, USA
[c] Brazilian Synchrotron Light Laboratory-LNLS, Rua Giuseppe Máximo Scolfaro, 10.000, Campinas, São Paulo 13083-970, Brazil

HIGHLIGHTS

- Interaction between ZnO NPs and γ-Al_2O_3 was investigated from neutral to alkaline pH.
- Zn-Al LDH could be formed under both near neutral and alkaline conditions.
- Formation of Zn-Al LDH is likely via a dissolution-sorption-coprecipitation process.
- This study helps to explain formation pathway of Zn-Al LDH in Zn/ZnO-contaminated environment.

GRAPHICAL ABSTRACT

Proposed reaction pathways for Zn-Al LDH formation. Blue, green, and red colors represent ZnO NPs, γ-Al_2O_3, and Zn-Al LDH, respectively.

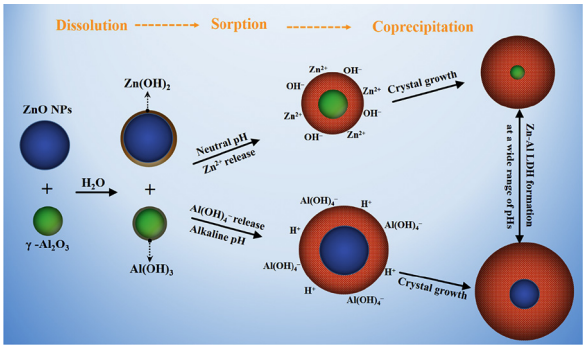

ARTICLE INFO

Article history:
Received 9 June 2018
Received in revised form 17 September 2018
Accepted 17 September 2018
Available online 19 September 2018

Editor: P Holden

Keywords:
ZnO nanoparticles
γ-Al_2O_3
Interaction
Layered double hydroxides
Transformation

ABSTRACT

Zinc and aluminum layered double hydroxides (Zn-Al LDH) are a common group of major Zn species in various Zn-contaminated soil/sediment environments, yet their formation pathways and underlying mechanisms under varied conditions are not well understood. This study investigated the formation of Zn-Al LDHs through the direct interaction of two solid substrates, ZnO nanoparticles (NPs) and a representative Al oxide, γ-Al_2O_3. Batch experiments and complementary microscopic and spectroscopic analyses were conducted to elucidate the reaction kinetics and mechanisms, as well as the morphologic and structural evolution of the products. Dissolved Zn and Al concentrations decreased significantly in a dual solid system compared to a single solid system. A bulk Zn-Al LDH phase was found to form under a wide pH range (6.5–9.5). Aside from Zn-Al LDH, γ-Al_2O_3 was the main remaining solid phase at pH 6.5, whereas ZnO NPs were the main residual solid phases at pH 9.5. Formation of amorphous $Zn(OH)_2$ was also observed at both pH values, likely due to Zn^{2+} release at low pH and $Al(OH)_4^-$ adsorption at high pH. It is proposed that the formation of Zn-Al LDH occurs via a dissolution-sorption-coprecipitation process, where the solubility of ZnO NPs or γ-Al_2O_3 solid phases determines the reaction pathways and kinetics under varied pH conditions. The results from this work revealed the transformation mechanisms for ZnO NPs under conditions from weakly acidic to alkaline pH with highly available Al particles and shed light on the environmental fate of ZnO NPs in Zn or ZnO NP contaminated environments.

* Corresponding author.
E-mail address: fxh73@mail.hzau.edu.cn (X. Feng).

https://doi.org/10.1016/j.scitotenv.2018.09.230
0048-9697/

1. Introduction

Engineered nanoparticles (ENPs) released into natural environments may interact with various constituents (e.g., microbes, minerals, natural organic matter) through an array of reactions such as redox transformation, homo/heteroaggregation, dissolution, and/or precipitation, which can subsequently impact their speciation, fate, transport, and bioavailability (Lowry et al., 2012; Wang et al., 2015). Understanding the kinetics and mechanisms of these processes is critical for evaluating the environmental behaviors and ecologic risks of ENPs (Lowry et al., 2012; Stark, 2011). Zinc oxide (ZnO) NPs are the second most produced group of ENPs and have widespread applications (e.g., catalysis, dye-sensitized solar cells, sunscreen products, textiles, and antibacterial agents) (Keller and Lazareva, 2014; Kołodziejczak-Radzimska and Jesionowski, 2014; Piccinno et al., 2012). These applications will inevitably lead to the release of ZnO NPs into natural environments (Keller and Lazareva, 2014), and studies have shown that their transport and retention in soils and sediments will strongly affect their potential exposure pathways and transformation (Hazeem et al., 2016; Li and Schuster, 2014; Sun et al., 2015). In addition, ZnO NP dissolution and transformation under the coexistence of environmentally relative ligands will remarkably alter the chemical form and thus the toxicity of ZnO NPs (Feng et al., 2016; Li et al., 2013; Ma et al., 2013). Recently, interaction of ZnO NPs with solid particles such as TiO_2 NP was reported to affect ZnO NPs transformation (Lv et al., 2014; Tong et al., 2014, 2015). However, there are very limited studies on the interaction of ENPs such as ZnO NPs with abundant natural mineral nanoparticles or colloids in the environment (Lv et al., 2014; Wang et al., 2015).

Aluminum (Al) (hydr)oxide minerals are ubiquitous in highly weathered environments and have been widely investigated in the fields of interfacial chemistry of nutrient elements and aqueous pollutants (Elzinga, 2012; Li et al., 2011, 2012; Siebecker et al., 2014; Yan et al., 2015). It has been commonly observed that Zn^{2+} and ZnO in soils enriched with Al (hydr)oxide or Al-bearing clay minerals can transform into less soluble Zn and Al layered double hydroxides (Zn-Al LDH) at relatively high initial metal concentrations (Jacquat et al., 2008, 2009; Nachtegaal et al., 2005; Voegelin et al., 2002, 2005, 2011; Voegelin and Kretzschmar, 2005). For example, formation of Zn-Al LDH in contaminated soils was found to be associated with samples with Zn content ranging from 571 to 20,476 mg kg^{-1} (Jacquat et al., 2009; Nachtegaal et al., 2005). Nearly pure Zn-rich phyllosilicate and Zn-LDH were identified at different locations within a single soil horizon, indicating that the availabilities of Al and Si controlled the type of precipitates formed (Jacquat et al., 2008). With the increase of Zn loading in soils, the percentage of precipitated Zn increased from 20 to 80%, while the precipitate type shifted from Zn-phyllosilicate at sites with lowest Zn content to predominantly Zn-LDH in heavily Zn-contaminated soils (Jacquat et al., 2008). Furthermore, Zn-bearing precipitates (Zn-LDH and Zn-rich phyllosilicates) became more dominant with the increase of pH and excessive total Zn content, relative to available adsorption sites (Jacquat et al., 2009). Zn-Al LDH was the most abundant Zn-precipitate in soils at pH 5.3–7.7, while Zn-rich phyllosilicates, less abundant than Zn-Al LDH, were also detected at lower soil pH (Jacquat et al., 2009). Previous studies have also revealed that the Zn^{2+} adsorbed on Al (hydro)oxide might continue to migrate into the crystal lattice of Al (hydro)oxide and formed new LDH phases at circumneutral pH values (Li et al., 2012; Miyazaki et al., 2013).

Although it is well known that there is a strong interaction between Zn^{2+} and Al (hydr)oxide or Al-contained clay minerals, less attention has been paid to the interaction of ZnO NPs with these Al-containing minerals. Voegelin et al. (2011) found that after four years of soil incubation, >90% of the added ZnO had transformed into Zn-Al LDH precipitate, with minor amounts of Zn-phyllosilicates and adsorbed Zn species in four soils, with pH ranging from acidic to alkaline. At acidic or neutral pH values, interaction of aqueous Zn^{2+} (derived from ZnO NPs dissolution) with Al-containing minerals accounts for the formation of Zn-Al LDH precipitate. However, at alkaline pH values where ZnO NPs are hardly soluble, the formation mechanisms of Zn-Al LDH are not clearly understood, despite the fact that such information is critical for understanding the environmental fate of ZnO NPs under circumneutral or alkaline pH conditions.

This study systematically investigated the interaction between ZnO NPs and γ-Al_2O_3 (a representative phase of highly reactive poorly crystalline Al oxide minerals) under varied pH conditions. Batch experiments were combined with a suite of complementary spectroscopy and microscopy analyses to reveal the reaction pathways and kinetics. Xu and Lu (2005) studied hydrothermal synthesis of layered double hydroxides (LDHs) from mixed MgO and Al_2O_3 for practical use as a material and explored LDH formation mechanisms under the less environmentally relevant conditions (i.e., high temperature, high pressure, and a long reaction time). Here, our study observed the rapid formation of Zn-Al LDH precipitates from the suspensions of ZnO and γ-Al_2O_3 mixtures at room temperature and atmospheric pressure and provided a quantitative and qualitative analysis of Zn-Al LDH in the products. Based on systematic instrumental characterization of the reaction products combined with wet chemistry analysis, this study further confirmed a dissolution-sorption-coprecipitation mechanism for the formation of Zn-Al LDH via two pathways at neutral and alkaline pH. Results from our study will enable better prediction of the transformation of ZnO NPs in natural environments and will provide implications for the interfacial behaviors of Zn or ZnO NPs in the environment.

2. Material and methods

2.1. Materials and its characterizations

ZnO NPs (99.9% purity) were obtained from Nanjing Emperor Nano Material Co., Ltd. (Nanjing, China). γ-Al_2O_3 was obtained from Sky Spring Nanomaterials Inc. (product #1328QI). Both materials were confirmed to be phase pure by X-ray diffraction (XRD) (Fig. S1). The average particle size of γ-Al_2O_3 determined by transmission electron microscopy (TEM), was approximately 5 nm (Figs. S2 and S3) (Feng et al., 2016; Yan et al., 2015). TEM also showed that ZnO NPs were mainly rhombohedral in shape, with an average particle size of 30 ± 10 nm and apparent lattice fringes of ~0.281 nm (Figs. S2 and S3). Brunauer-Emmett-Teller (BET) specific surface areas for γ-Al_2O_3 and ZnO NPs were 325 and 37 m^2 g^{-1}, respectively. More details of these materials can be found in our previous publications (Feng et al., 2016; Yan et al., 2015).

2.2. Batch experiments

Dissolution kinetics of ZnO NPs (0.81 g L^{-1}) or γ-Al_2O_3 (0.51 g L^{-1}) was conducted in 0.01 M KCl solution at pH 6.5–9.5. ZnO NPs (0.162 g) and γ-Al_2O_3 (0.102 g) were weighed and mixed several times in a weigh boat, using disposable polypropylene spatulas. Then, the mixture was added to 200 mL of a 0.01 M KCl solution that was preadjusted to different pH values (6.5, 7.5, 8.5, and 9.5). The pH of the reaction suspension was maintained constant using a pH-stat titrator (Metrohm 907 Titrando, Switzerland). The molar ratio of ZnO:γ-Al_2O_3 is 2:1. The reaction temperature was maintained at 25 ± 0.2 °C using a water bath. At certain time points, aliquots of the reaction suspension were syringe filtered (0.22 μm). The filtrate was analyzed for total Zn concentrations using an atomic absorption spectrometer (Varian 240FS). Additionally, total Al concentration was determined using a spectrophotometric method based on the reaction of Al with chrome azurol S (Pakalns, 1965; Tóth et al., 2004). A portion of the suspensions was also centrifuged (9500 ×g, 10 min), washed twice with 0.01 M KCl solution at corresponding pH, and the wet pastes were evenly spread in a petri dish and dried under air flow at room temperature. Dried solids were finely ground and analyzed for their morphological and structural characteristics (see below). All experiments were conducted in duplicate.

2.3. Characterization of reaction products

The reaction products were characterized using a suite of complementary techniques, including X-ray diffraction (XRD), Fourier transform infrared spectroscopy (FTIR), scanning and transmission electron microscopy (SEM/TEM), ^{27}Al nuclear magnetic resonance (NMR) spectroscopy, and Zn K-edge extended X-ray absorption spectroscopy (EXAFS). Experimental details of XRD, FRIT, SEM, and TEM analyses are provided in the Supplementary data.

2.3.1. ^{27}Al NMR

Solid state ^{27}Al single-pulse MAS (SP/MAS) NMR analysis of the reaction products was conducted on a 400 MHz NMR spectrometer (9.4 T) (Bruker Advance III 400 M, Switzerland) operated at 130.2 MHz, using a 5-mm PABBO BB-1 H/D Z-GRD probe at a spinning rate of 12 kHz. A 6 μs 90° pulse was calibrated using a 1.0 M $Al(NO_3)_3$ solution standard, but only 1 μs rf (radio frequency) pulse length was chosen for measuring the solid samples. Pulse delay was optimized as 5 s, and approximately 250 scans were collected for each sample. The ^{27}Al chemical shifts (δ_{Al}) are reported relative to an external 1.0 M $Al(NO_3)_3$ solution set to $\delta_{Al} = 0$ ppm.

2.3.2. Zn K-edge EXAFS

50 mg of air dried samples was mixed with 50 mg of boron nitride (BN), and then finely ground, pressed into pellets, and mounted on a sample holder covered with Kapton tape. Zinc K-edge EXAFS data were collected at Beamline XAFS2 of the Brazilian Synchrotron Light Laboratory (LNLS) (Campinas, Brazil) and at Beamline 1W1B of the Beijing Synchrotron Radiation Facility (BSRS) (Beijing, China). ZnO NPs, synthetic $Zn(OH)_2$ and Zn-Al LDH were used as reference compounds (Yan et al., 2018). Data collection was conducted in transmission mode, using a Zn foil for energy calibration setting E_0 at the Zn K-edge (9659 eV). Data analysis used the DEMETER software package (Ravel and Newville, 2005). Linear combination fitting (LCF) of Zn EXAFS data was performed using the ZnO NPs and LDH reference compounds at *k* space of 2.2–12.5 $Å^{-1}$.

3. Results and discussion

3.1. Dissolution kinetics

To explore the interaction between ZnO NPs and γ-Al_2O_3 (dual solid system) under varied pH conditions, the first step was to examine the stability of these two solid phases alone (single solid system) at corresponding pH values. The dissolution kinetics of ZnO NPs and γ-Al_2O_3 (single solid system) at pH 6.5–9.5 are shown in Fig. S4. Dissolution of ZnO NPs increased with decreasing pH, with a much greater extent of dissolution at pH 6.5 (~6.36 mM dissolved Zn^{2+} at 48 h, equivalent to ~63.6% of total Zn) than that at pH 7.5–9.5 (<0.5 mM dissolved Zn^{2+} at 48 h) (Fig. S4a). In contrast, the dissolution of γ-Al_2O_3 was enhanced by increasing pH. Dissolved Al(III) concentration increased rapidly at pH 9.5, while limited dissolution of γ-Al_2O_3 was observed at pH 6.5 and 7.5. At 48 h, dissolved Al(III) concentrations at pH 9.5, 8.5, 7.5 and 6.5 were ~60, 17, 3, and 0.2 μM (corresponding to 0.6, 0.17, 0.03 and 0.02% of total γ-Al_2O_3), respectively (Fig. S4b).

When ZnO NPs and γ-Al_2O_3 were reacted together (i.e. dual solid system), the concentration of dissolved Zn^{2+} also decreased with increasing pH and became negligible at pH 8.5 and 9.5 (Fig. 1a). This overall trend was similar to the system with ZnO NPs alone (i.e., single solid system). However, the equilibrium concentration of dissolved Zn^{2+} at 48 h was only ~2.35 mM (23.5% of total ZnO NPs), much lower than that of the ZnO NPs experiment (~6.36 mM). The dissolution kinetics of γ-Al_2O_3 in the dual solid system also showed a pH-dependent trend similar to the system with γ-Al_2O_3 alone, but with a much lower equilibrium dissolved Al(III) concentration (~5 μM at pH 9.5, 0.05% of total γ-Al_2O_3) (Fig. 1b). Compared to single solid systems, such a remarkable decrease in both dissolved Zn^{2+} and Al(III) concentrations in the dual solid system suggests the potential formation and/or transformation of solid phases. Therefore, a suite of complementary techniques was utilized to characterize the chemical, morphological, and structural properties of the reacted solid phases, as detailed below.

3.2. Mineralogical transformation and morphological evolution

XRD revealed the formation of Zn-Al LDH in the reacted dual solid system. The intensity of the peaks corresponding to the Zn-Al LDH phase was also pH-dependent, i.e., more significant at pH 6.5 than pH 7.5–9.5 (Fig. 2). At pH 6.5, although the diffraction peaks of ZnO NPs were still observed after 2 h of reaction, they had almost completely disappeared and the diffraction peaks of Zn-Al LDH became dominant after 12 h of reaction, consistent with the previous report that Zn-Al LDH can form within 15 min upon Zn^{2+} sorption onto γ-Al_2O_3 (Li et al., 2012). In contrast, for reactions conducted at pH 7.5–9.5, no observable difference in the XRD patterns was found for the reaction products at different reaction times from 2 h to 2 d. The Zn-Al LDH diffraction peaks at ~11 and ~23°, as indexed with (003) and (006) for a rhombohedral symmetry (3R) (Xu and Lu, 2005), were pronounced in all reaction samples. Those at ~35, ~39, and ~46° can be indexed as the (012), (015), and (018) faces of Zn-Al LDH, respectively (Figs. 2 and S1a) (Li et al., 2012; Xu and Lu, 2005). The formed LDH is more likely a $3R_1$-polytype LDH phase (featured mainly by the diffraction peaks of (012), (015), (018) faces), instead of a $3R_2$-polytype LDH phase

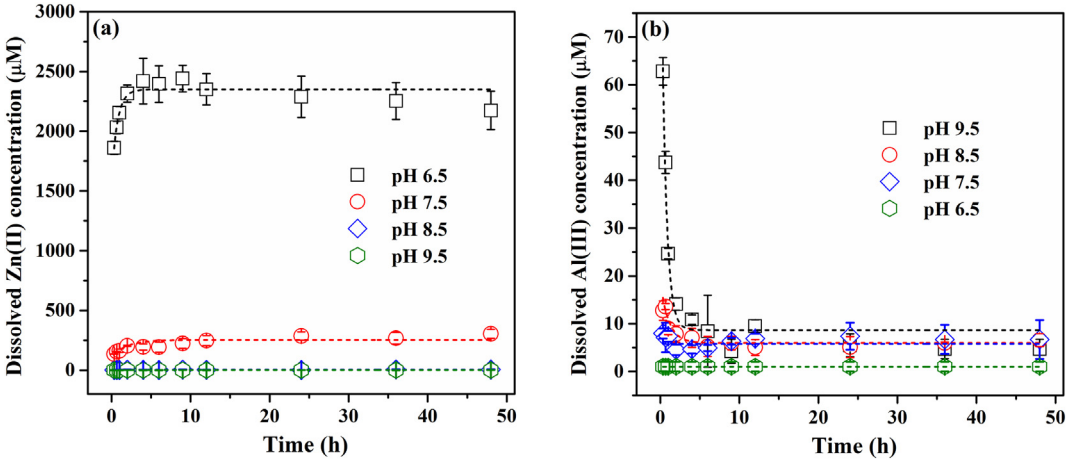

Fig. 1. Concentration of dissolved Zn(II) (a) and Al(III) (b) at different pH values during the reaction of ZnO NPs and γ-Al_2O_3.

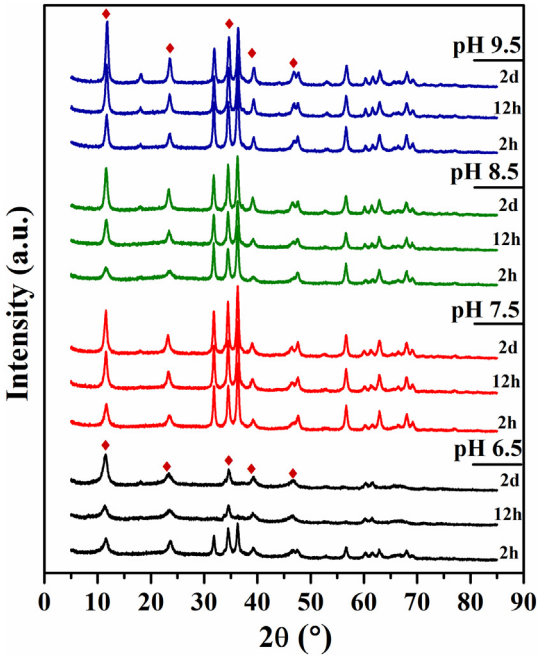

Fig. 2. XRD patterns of ZnO NPs and γ-Al_2O_3 reaction products at different reaction times (2 h, 12 h, and 2 d) and pH 6.5–9.5. Red diamond symbols indicate the (003), (006), (012), (015), and (018) planes of Zn-Al LDH, from left to right. (For interpretation of the references to color in this figure legend, the reader is referred to the web version of this article.)

(featured mainly by the diffraction peaks of (014), (017), (0,1,10) faces) (Xu and Lu, 2005).

The IR bands at 3442, 1644, and 1130 cm^{-1} belong to the ν(OH) and δ(OH) of water molecules, and the δ(OH) of bridged Al—OH, respectively (Fig. S5) (Dambournet et al., 2008). The IR bands at 773 and 616 cm^{-1} can be attributed to the vibration of the AlO_4 tetrahedra and AlO_6 octahedra (Saniger, 1995; Tarte, 1967). The infrared absorption peaks at approximately 1364 and 1405 cm^{-1} can be assigned to the stretching vibration of CO_3^{2-} adsorption in the interlayer region of Zn-Al LDH and of CO_3^{2-} adsorption at the surface sites of solids (e.g., residual ZnO NPs, residual γ-Al_2O_3, and newly formed Zn-Al LDH), respectively (Li et al., 2012; Xu and Lu, 2005). A shoulder peak at 3110 cm^{-1} can be attributed to OH stretching in H-bonded OH—CO_3^{2-} in the FTIR spectra of all samples, which is more obvious for pH 9.5 products (Fig. S5) (Xu and Lu, 2005). These results suggest that the newly formed Zn-Al LDH phase contains some CO_3^{2-}, possibly via the absorption of CO_2 from air and the subsequent reaction with water to form HCO_3^- or CO_3^{2-}. The peak for interlayer CO_3^{2-} (at 1355 cm^{-1}) becomes more obvious at higher pHs (Fig. S5), likely due to the higher uptake of CO_2 from air and resulting in carbonate species (Xu and Lu, 2005).

SEM and TEM images showed that the unreacted γ-Al_2O_3 phase had an average particle size of ~5 nm, and unreacted ZnO NPs were mainly rhombohedral with an average particle size of ~30 nm (Figs. S2 and S3). After the reaction of ZnO NPs and γ-Al_2O_3 at pH 6.5 and 9.5, precipitates with flake morphology and >200 nm size were observed in both SEM and TEM images of the reaction products (Fig. 3). These precipitates can be identified as the Zn-Al LDH phase from their typical flaky morphology, similar to the well-defined hexagonal flaky morphology of LDHs synthesized from hydrothermal treatment and coprecipitation (Li et al., 2012; Pushparaj et al., 2015). SEM and TEM analyses (Fig. 3) also revealed that the edges and surfaces of Zn-Al LDH formed at pH 9.5 were smoother than those formed at pH 6.5. The lack of well-defined hexagonal LDH morphology was also observed in previous investigations (Zn-Al-Cl and Zn-Al-NO_3 LDHs) and is possibly the result of a higher Al content in Zn-Al LDH (Pushparaj et al., 2015). The fact that fine and small γ-Al_2O_3 particles were abundantly present at pH 6.5 and large ZnO sphere particles were relatively abundant at pH 9.5 (Fig. 3) is consistent with XRD results that ZnO diffraction peaks persisted at high pH (Fig. 2).

Combined XRD and electron microscopy evidence suggests that pH plays a critical role in the dissolution of ZnO and γ-Al_2O_3 NPs, as well as the subsequent morphology and structure of the formed Zn-Al LDH, and that the formation pathways of Zn-Al LDH at different pH values may also be different.

3.3. Structure transformation

Zn EXAFS and ^{27}Al NMR spectroscopy were applied to further investigate the phase and structural evolution of the system and the underlying reaction mechanisms. XRD results can provide only limited structural information with regard to Al in this system, as γ-Al_2O_3 is poorly crystalline and lacks strong diffraction signals (Fig. S1b) (Li et al., 2012; Yan et al., 2015). Zn EXAFS can reveal the coordination environment (Li et al., 2012; Lv et al., 2012; Trainor et al., 2000). ^{27}Al NMR spectroscopy is the most common technique for characterizing the Al chemical environment.

The ^{27}Al NMR spectrum of raw γ-Al_2O_3 showed two peaks at chemical shifts of +65 and +9.4 ppm, which can be assigned to Al in tetrahedral (AlO_4) and octahedral coordination (AlO_6), respectively (Fig. 4) (Li et al., 2012; Miyazaki et al., 2013; Pushparaj et al., 2015; Yan et al., 2014). Due to the formation of Zn-Al LDH precipitates, it was expected that a single Zn vacancy would affect the six neighboring Al atoms, whereas Zn substitution at an Al site affects three neighboring Al atoms which would otherwise change the chemical shifts of octahedral AlO_6 in NMR spectrum by approximately 4–5 ppm (Li et al., 2012; Miyazaki et al., 2013; Pushparaj et al., 2016). Fig. 4 shows that a new peak at 13.91 ppm appeared in the NMR spectra of the reaction products from all pH conditions, which can be attributed to octahedral AlO_6 in Zn-Al LDH phase (Li et al., 2012; Pushparaj et al., 2016). In all reaction products, the peak intensity of both AlO_4 tetrahedra ($\delta_{Al\text{-}27}$ = +65 ppm) and AlO_6 octahedra ($\delta_{Al\text{-}27}$ = +9.4 ppm) in γ-Al_2O_3 decreased, and the peak intensity of AlO_6 octahedra ($\delta_{Al\text{-}27}$ = +13.91 ppm) in the Zn-Al LDH increased (Fig. 4b and c), suggesting that octahedral Al in Zn-Al LDH precipitates may come from both tetrahedral and octahedral Al from γ-Al_2O_3 transformation. As the pH increased from 6.5 to 9.5, the chemical shift at $\delta_{Al\text{-}27}$ = +65 and 9.5 ppm decreased gradually, but remained present in NMR spectra of the reaction products, indicating that the dissolution of γ-Al_2O_3 was facilitated by increasing pH. However, some γ-Al_2O_3 was still present in the reaction products, in agreement with SEM and TEM observations, but was difficult to detect by XRD, due to its amorphous nature and weak diffraction peaks.

As shown in Fig. 5, in the Zn K-edge XANES spectra there were four peaks at 9666.4, 9676.7, 9711.7 and 9735.9 eV characterizing ZnO NPs; four peaks at 9664.9, 9682, 9705.7 and 9717.1 eV that are diagnostic features of Zn-Al LDH; and four peaks at 9665, 9679.9, 9705.5 and 9714.9 eV for $Zn(OH)_2$. The Zn XANES spectra showed that ZnO NPs (with Zn in tetrahedral ZnO_4 coordination) were partially transformed into Zn-Al LDH (mainly containing Zn in octahedral ZnO_6 coordination) and some $Zn(OH)_2$ (Fig. 5). To quantify the relative percentage of different Zn species, Zn K-edge EXAFS spectra of the solid products from different pH conditions and reactions time were analyzed by linear combination fitting (LCF) using ZnO NPs, $Zn(OH)_2$, and Zn-Al LDH as end members (Figs. 6, S6 and S7). The LCF results indicated that the amount of Zn-Al LDH increased with increasing solution pH and reaction time (Fig. 6; Table S1). Additionally, $Zn(OH)_2$ comprised approximately 20% of all reaction products, as revealed by LCF of Zn EXAFS (Table S1), likely existing as an amorphous phase, due to the lack of $Zn(OH)_2$ peaks in XRD patterns (Fig. 2). LCF results of the final products

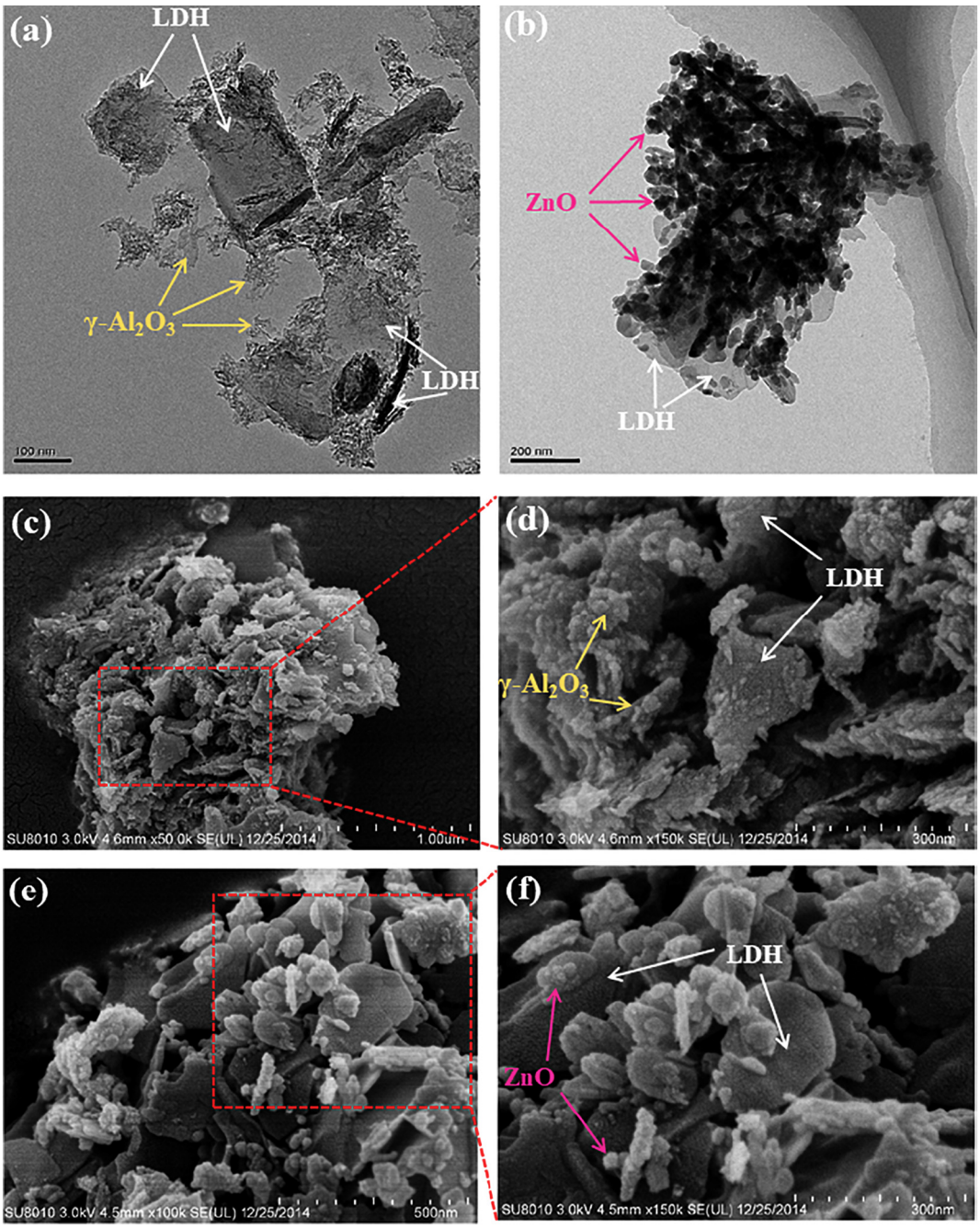

Fig. 3. TEM and SEM images of ZnO NPs and γ-Al_2O_3 reaction products after 2 d at pH 6.5 (a, c) and pH 9.5 (b, e), as well as corresponding zoomed SEM views of selected regions (red lines) (d) and (f), respectively. (For interpretation of the references to color in this figure legend, the reader is referred to the web version of this article.)

at different pH (6.5, 7.5, 8.5, and 9.5) (Fig. 6a) revealed that Zn-Al LDH accounts for 78.6, 34.3, 44.8, and 51.3% of the total Zn in the solid phase, respectively. Considering that 21.7% of the total Zn is soluble Zn^{2+} in the aqueous phase, it can be estimated that 61.5% of total Zn in the system was transformed into Zn-Al LDH at pH 6.5 after 48 h of reaction (Table S1). Similarly, 33.3, 44.8, and 51.3% of total Zn from ZnO NPs transformed into Zn-Al LDH at pH 7.5, 8.5, and 9.5, respectively (Table S1). Solid phases of reactions at pH 6.5 and 9.5 were collected at different time points (2, 12, 48 h) and the LCF results were also compared (Fig. 6b). The fitting results showed that the relative abundance of Zn-Al LDH in the systems increased from 36.9 to 61.5% at pH 6.5 and from 25.2 to 51.3% at pH 9.5, as the reaction time increased from 2 to 48 h (Table S1), suggesting a faster transformation at pH 6.5.

3.4. Reaction pathways of Zn-Al LDH formation

Previous studies have shown that the formation of Zn-Al LDH and Zn adsorption/complexation are important pathways for the accumulation of massive amounts of Zn in soils, when pH is high and Zn loading exceeds the adsorption capacity of soil (Voegelin et al., 2005, 2011). In this study, combined XRD, SEM, TEM, EXAFS, and NMR analyses revealed the formation of crystalline Zn-Al LDH precipitates during the interaction between ZnO NPs and γ-Al_2O_3 at different pH. The underlying reaction pathways of Zn-Al LDH precipitate formation under various conditions are further discussed below.

Li et al. (2012) demonstrated that Zn^{2+} sorption onto γ-Al_2O_3 led to the formation of a crystalline Zn-Al LDH phase. It has also recently been reported that $Al(OH)_4^-$ can enter into the $Zn(OH)_2$ structure,

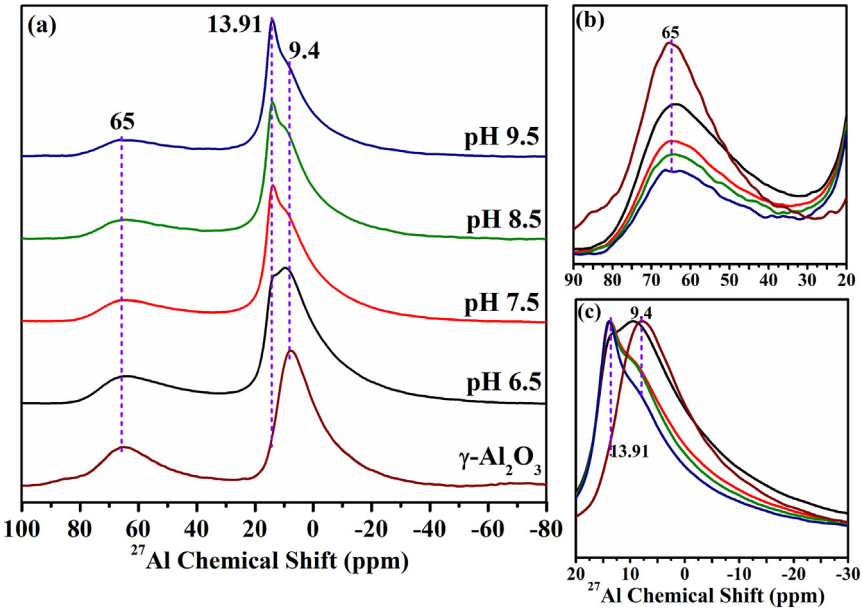

Fig. 4. (a) ^{27}Al SP/MAS NMR analysis of unreacted γ-Al_2O_3, as well as ZnO NPs and γ-Al_2O_3 reaction products after 2 d at pH 6.5–9.5; (b) zoomed view (+20 to +90 ppm) showing tetrahedrally coordinated Al; (c) zoomed view (−30 to +20 ppm) showing octahedrally coordinated Al.

replace Zn^{2+} with Al^{3+}, and enhance transformation of the solid phase into Zn-Al LDH by creating positive charges in the $Zn(OH)_2$ solid phase (Meng et al., 2017). Considering the high solubility of ZnO NPs at neutral pH and γ-Al_2O_3 at alkaline pH (Figs. 1 and S4), and the fact that the main dissolved species of Zn(II) and Al(III) were Zn^{2+} at pH 6.5 and $Al(OH)_4^-$ at pH 9.5, respectively (Fig. S8), the dissolved Zn^{2+} or $Al(OH)_4^-$ played a critical role in the formation of the Zn-Al LDH phase at experimentally different pH. We propose that a dissolution-sorption-coprecipitation process might have occurred at neutral and alkaline pH, when concentrations of dissolved Zn^{2+} or $Al(OH)_4^-$ in solution were high enough to drive the formation of the Zn-Al LDH phase. Before or during the formation of Zn-Al LDH, the hydrolysis of ZnO NPs and γ-Al_2O_3 and the dissociation of $Zn(OH)_2$ and $Al(OH)_3$ (Eqs. (1) and (2)) may occur at the surface of the solid particles (Bian et al., 2011; Xu and Lu, 2005; Zhang et al., 2018). Then dissolved Zn^{2+} and $Al(OH)_4^-$ may be incorporated into the hydrolyzed γ-Al_2O_3 and ZnO thin layer, respectively, to form Zn-Al LDH at neutral and alkaline pH (Eqs. (3) and (4)). These reaction pathways are simplified to the following equations:

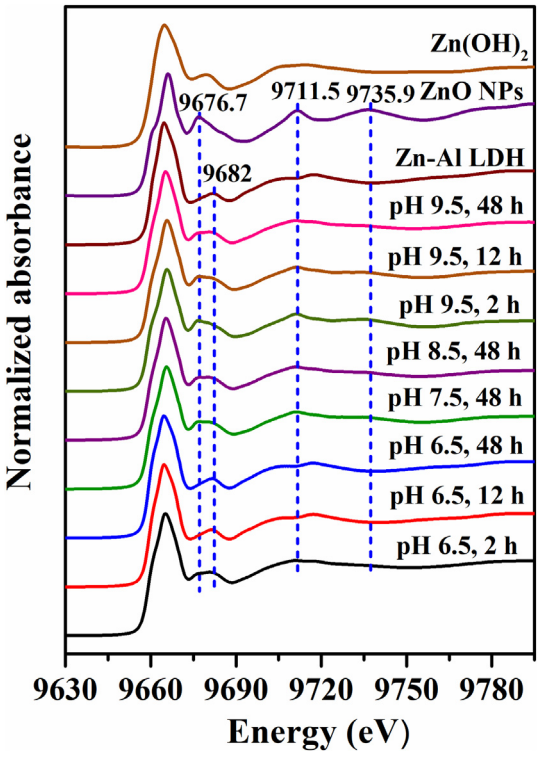

Fig. 5. Zn K-edge XANES spectra of ZnO NPs and γ-Al_2O_3 reaction products at different pH, as well as the powder standards for qualitative comparison.

$$\gamma Al_2O_{3(s)} + 3H_2O \leftrightarrow 2Al(OH)_{3(s)} + 2H_2O \leftrightarrow 2Al(OH)_4^- + 2H^+ \quad (1)$$

$$ZnO_{(s)} + H_2O \leftrightarrow Zn(OH)_{2(s)} \leftrightarrow Zn^{2+} + 2OH^- \quad (2)$$

$$xZn^{2+} + Al(OH)_{3(s)} + (2x + a - 1)H_2O + Cl^- \leftrightarrow Zn_xAl(OH)_{2x+2}Cl \cdot aH_2O_{(s)} + (2x-1)H^+ \quad (3)$$

$$xZn(OH)_{2(s)} + Al(OH)_4^- + aH_2O + Cl^- \leftrightarrow Zn_xAl(OH)_{2x+2}Cl \cdot aH_2O_{(s)} + 2OH^- \quad (4)$$

The freshly generated $Zn(OH)_{2(s)}$ and $Al(OH)_{3(s)}$ phases first formed thin layers on the corresponding oxide particle surfaces. These hydroxide layers were then dissolved to release Zn^{2+} at pH 6.5 or $Al(OH)_4^-$ at pH 9.5, which can lead to the continuous hydrolysis of the corresponding oxides. Then, dissolved Zn^{2+} or $Al(OH)_4^-$ can incorporate into the hydrolyzed γ-Al_2O_3 or ZnO thin surface layer to further facilitate the dissolution-sorption-coprecipitation processes. These reactions can be substantiated by the dynamics of OH^- and H^+ release during the process (Fig. S9). A previous study reported that the formation of Mg-Al LDH resulted in the increase of solution pH (from 7 to 10.1 or 11.5 to 11.8) due to the incorporation of dissolved Mg^{2+} or $Al(OH)^{4-}$ into the solid γ-Al_2O_3 or MgO surface (Xu and Lu, 2005). Here, the dynamics of OH^- and H^+ release at pH 6.5 and 9.5 were quantified by measuring the amount of HCl or KOH consumed following a reported procedure (Feng et al., 2016). A rapid release of OH^- was observed at both pH 6.5 and 9.5 during the initial 6 h, although the released amount was much higher at pH 6.5 (~3.85 mM compared to ~0.85 mM at

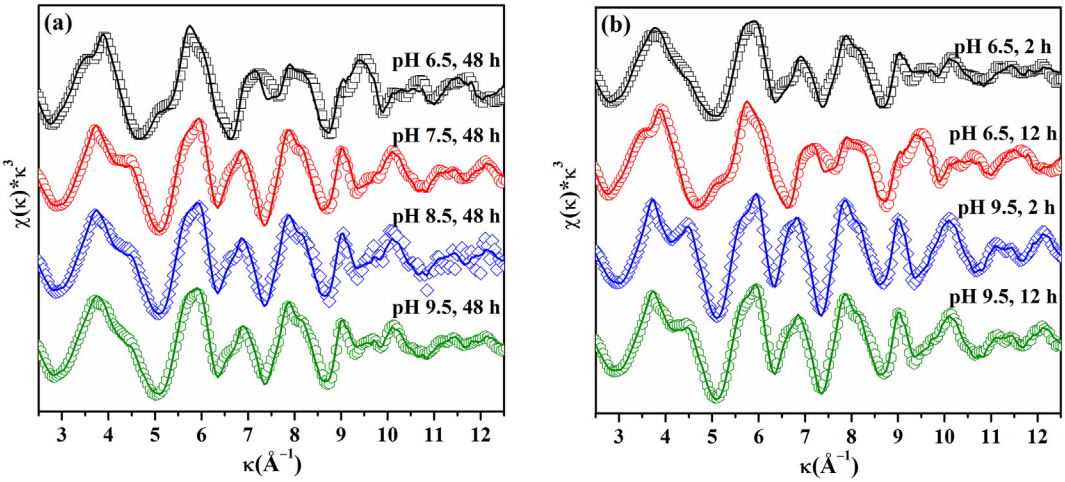

Fig. 6. Zn K-edge EXAFS spectra (open cycle) and linear combination fitting (LCF) results (solid lines) of ZnO and γ-Al_2O_3 reaction products (a) at different pH at 2 d and (b) at different reaction times (2 and 12 h) at pH 6.5 and 9.5. The number in the parentheses is the percentage of Zn-Al LDH in the final solids, based on LCF.

pH 9.5). It is highly likely that in the initial reaction stage at pH 6.5 release of OH^- during the hydrolysis/dissolution of ZnO NPs (Eq. (2)) outpaced the release of H^+ during Zn^{2+} incorporation into LDH (Eq. (3)). As the reactions proceeded (beyond 12 h), the release of H^+ due to predominant Zn-Al LDH formation via Zn^{2+} adsorption/incorporation in the later reaction stage may have exceeded that of OH^- release due to ZnO dissolution. Based on both XRD and Zn EXAFS results, beyond 12 h, ZnO NPs were mostly dissolved and transformed into Zn-Al LDH (Figs. 2 and 5). At pH 9.5, the release of OH^- was likely from the incorporation of $Al(OH)_4^-$ into the hydrolyzed ZnO thin layer (Eq. (4)). Although $Al(OH)_4^-$ production via hydrolysis of $Al(OH)_3$ led to H^+ release (Eq. (1)), the net release of OH^- was also achieved in the initial reaction stage (though much less than that at pH 6.5), likely due to the high rate of Zn-Al LDH formation at pH 9.5. The decrease in the formation rate of Zn-Al LDH and the relatively enhanced surface alkali ionization of residual γ-Al_2O_3 or ZnO NPs could account for the net H^+ release after 10 h of reaction (Uekawa et al., 2004; Xu and Lu, 2005). To obtain further information on pH variation at the comparison, we have conducted a series of pH-uncontrolled experiments. With initial pH values of 6.5, 7.5, 8.5 and 9.5, the final pH values were 7.5, 7.6, 7.8, 8.0 for ZnO NPs suspensions, and 6.4, 7.2, 7.9, 8.3 for γ-Al_2O_3 suspensions, respectively.

It is indicated that migration of Al from γ-Al_2O_3 to the precipitates is critical for the formation of secondary Zn-Al LDH phases with Zn^{2+} at pH 7.5 (Li et al., 2012). In addition, the much higher surface area and reactivity of γ-Al_2O_3 compared to other Al (hydr)oxide phases can facilitate the surface hydrolysis of γ-Al_2O_3 and the formation of Zn-Al LDH. Recently, Gou et al. (2018) proposed that Zn adsorbed onto the Al oxide surface at pH of 6.0–6.5 and/or Zn concentrations of 0.1–0.2 mM occurred as an inner-sphere surface complex ($\Gamma < 0.8\ \mu mol\ m^{-2}$) and resulted in a $\Delta^{66}Zn_{sorbed\text{-}aqueous}$ fractionation of $+0.47 \pm 0.03‰$ between the solid and aqueous phases. And at Zn concentrations of 0.4–0.8 mM and pH of 7.0–7.5, the precipitated Zn in the Zn-Al LDH phase was present as an octahedron surrounded by 6 oxygen atoms and explained little about the Zn isotope fractionation between the two phases. In contrast with other minerals, the consistency in the Zn isotope fractionation factors implied that the coordination number for the first shell has the dominant isotopic effect over the nature of the secondary shells for the sorbed Zn on mineral surfaces. Bond length and structural order contributed significantly to the isotopic fractionation of Zn during its sorption on metal oxides (Gou et al., 2018). In our study, the dissolved Zn concentration was able to reach 0.8 mM within first few minutes at pH 6.5 (Fig. 1a), which may explain the observation of Zn-Al LDH formation at this pH. It has also been reported that adsorption of Zn^{2+} onto the $Al(OH)_3$ gel induced Al^{3+} dissolution, followed by the coprecipitation of Al^{3+} with Zn^{2+} (as AlO_4 tetrahedral structures) on the surface of $Al(OH)_3$ gel (Miyazaki et al., 2013). However, in our study, the abundance of tetrahedral AlO_4 in γ-Al_2O_3 decreased (Fig. 4), consistent with the report of Li et al. (2012). Additionally, ~20% of the $Zn(OH)_2$ in the LCF results may be due to the incomplete transformation of ZnO into Zn-Al LDH at ambient temperature, which led to the formation of minor amounts of $Zn(OH)_2$. It was reported that Zn-Al LDH samples prepared by the coprecipitation method, with careful pH control and hydrothermal treatment, were found to produce Zn-Al LDH precipitates with highly ordered local structures and good crystallinity (large particle size) (Pushparaj et al., 2015). Thus, temperature might be an important factor for controlling the transformation of ZnO and the formation of Zn-Al LDH. Meanwhile, this study found that the edges and surfaces of Zn-Al LDH formed at pH 9.5 were smoother than those formed at pH 6.5, based on SEM and TEM observations (Fig. 3). Therefore, pH seems to also play a critical role in the crystallinity of the formed Zn-Al LDH, with LDH formed at natural pH having a lower structure order or smaller crystallite size. Furthermore, the presence of anions was thought to also have a remarkable impact on the formation and local structure of Zn-Al LDH phases (Pushparaj et al., 2015, 2016).

4. Conclusions and perspectives

This study combined batch measurements and solid phase characterizations, using a suite of spectroscopy and microscopy techniques and revealed the formation of Zn-Al LDH through direct interaction between ZnO and γ-Al_2O_3 NPs at various pH. The formation of Zn-Al LDH likely occurred via a dissolution-sorption-coprecipitation pathway. In the material science field, a similar LDH formation pathway through interaction between MgO and Al_2O_3 NPs under hydrothermal conditions was reported, and the studied reaction conditions had little environmental relevance (Xu and Lu, 2005). Here, the reaction kinetics and mechanism of LDH formation revealed by our study will provide implications for the formation of Zn-Al LDH under environmentally relevant conditions such as soils/sediments sites with ZnO/Zn^{2+} contamination. Similar reactions between active solid particles, abundant in soil or sediment systems, can occur extensively and affect their transformation, speciation, environmental behaviors, and ecological risks. This study used γ-Al_2O_3 as a representative Al phase, but the potential difference between this phase and other Al-containing phases should be further investigated. Meanwhile, considering the complexity of geochemical processes in the natural environments, further studies should be conducted to evaluate the effects of other parameters, such as particle size, mineral type, ratio of Zn and Al in the initial metal oxide mixture, reaction temperature, solution chemistry (e.g., presence of complexing

anions such as Cl^-, CO_3^{2-}, SO_4^{2-} and PO_4^{3-}), low molecular weight organic acids, and natural organic matter.

Acknowledgements

The authors gratefully acknowledge supports from the National Natural Science Foundation of China (Grant Nos. 41603100 and 41471194), and the Strategic Priority Research Program of the Chinese Academy of Sciences (No. XDB15020402). R.H. and Y.T. acknowledge support from National Science Foundation under Grant Nos. 1739884 and 1559087. The authors thank the Associate Editor, Dr. Patricia Holden, and three reviewers for thoughtful thorough reviews and constructive comments. Use of beamline XAFS2 of the Brazilian Synchrotron Light Laboratory was granted through the research proposal under Contract No. XAFS1-17041.

Appendix A. Supplementary data

Supplementary data related to this article includes XRD patterns, TEM and SEM images of unreacted ZnO NPs and γ-Al_2O_3; the XRD pattern of synthesized Zn-Al LDH; FTIR and EXAFS spectra of the reaction products and reference compounds; dissolution kinetics and accumulation kinetics of OH^-; equilibrium solubility diagram of ZnO and γ-Al_2O_3. Supplementary data to this article can be found online at doi: https://doi.org/10.1016/j.scitotenv.2018.09.230.

References

Bian, S.W., Mudunkotuwa, I.A., Rupasinghe, T., Grassian, V.H., 2011. Aggregation and dissolution of 4 nm ZnO nanoparticles in aqueous environments: influence of pH, ionic strength, size, and adsorption of humic acid. Langmuir 27, 6059–6068.

Dambournet, D., Demourgues, A., Martineau, C., Pechev, S., Lhoste, J., Majimel, J., Vimont, A., Lavalley, J.-C., Legein, C., Buzaré, J.-Y., Fayon, F., Tressaud, A., 2008. Nanostructured aluminium hydroxyfluorides derived from β-AlF_3. Chem. Mater. 20, 1459–1469.

Elzinga, E.J., 2012. Formation of layered Fe(II)–Al(III)-hydroxides during reaction of Fe(II) with aluminum oxide. Environ. Sci. Technol. 46, 4894–4901.

Feng, X., Yan, Y., Wan, B., Li, W., Jaisi, D.P., Zheng, L., Zhang, J., Liu, F., 2016. Enhanced dissolution and transformation of ZnO nanoparticles: the role of inositol hexakisphosphate. Environ. Sci. Technol. 50, 5651–5660.

Gou, W., Li, W., Ji, J., Li, W., 2018. Zn isotope fractionation during sorption on Al oxide: atomic level understanding from EXAFS. Environ. Sci. Technol. 2018 (52), 9087–9096.

Hazeem, L.J., Bououdina, M., Rashdan, S., Brunet, L., Slomianny, C., Boukherroub, R., 2016. Cumulative effect of zinc oxide and titanium oxide nanoparticles on growth and chlorophyll a content of *Picochlorum* sp. Environ. Sci. Pollut. Res. 23, 2821–2830.

Jacquat, O., Voegelin, A., Villard, A., Marcus, M.A., Kretzschmar, R., 2008. Formation of Zn-rich phyllosilicate, Zn-layered double hydroxide and hydrozincite in contaminated calcareous soils. Geochim. Cosmochim. Acta 72, 5037–5054.

Jacquat, O., Voegelin, A., Kretzschmar, R., 2009. Soil properties controlling Zn speciation and fractionation in contaminated soils. Geochim. Cosmochim. Acta 73, 5256–5272.

Keller, A.A., Lazareva, A., 2014. Predicted releases of engineered nanomaterials: from global to regional to local. Environ. Sci. Technol. Lett. 1, 65–70.

Kołodziejczak-Radzimska, A., Jesionowski, T., 2014. Zinc oxide—from synthesis to application: a review. Materials 7, 2833–2881.

Li, L., Schuster, M., 2014. Influence of phosphate and solution pH on the mobility of ZnO nanoparticles in saturated sand. Sci. Total Environ. 472, 971–978.

Li, W., Harrington, R., Tang, Y., Kubicki, J.D., Aryanpour, M., Reeder, R.J., Parise, J.B., Phillips, B.L., 2011. Differential pair distribution function study of the structure of arsenate adsorbed on nanocrystalline γ-alumina. Environ. Sci. Technol. 45, 9687–9692.

Li, W., Livi, K.J.T., Xu, W., Siebecker, M.G., Wang, Y., Phillips, B.L., Sparks, D.L., 2012. Formation of crystalline Zn–Al layered double hydroxide precipitates on γ-alumina: the role of mineral dissolution. Environ. Sci. Technol. 46, 11670–11677.

Li, M., Lin, D., Zhu, L., 2013. Effects of water chemistry on the dissolution of ZnO nanoparticles and their toxicity to *Escherichia coli*. Environ. Pollut. 173, 97–102.

Lowry, G.V., Gregory, K.B., Apte, S.C., Lead, J.R., 2012. Transformations of nanomaterials in the environment. Environ. Sci. Technol. 46, 6893–6899.

Lv, J., Zhang, S., Luo, L., Han, W., Zhang, J., Yang, K., Christie, P., 2012. Dissolution and microstructural transformation of ZnO nanoparticles under the influence of phosphate. Environ. Sci. Technol. 46, 7215–7221.

Lv, J., Zhang, S., Wang, S., Luo, L., Huang, H., Zhang, J., 2014. Chemical transformation of zinc oxide nanoparticles as a result of interaction with hydroxyapatite. Colloids Surf. A 461, 126–132.

Ma, H., Williams, P.L., Diamond, S.A., 2013. Ecotoxicity of manufactured ZnO nanoparticles – a review. Environ. Pollut. 172, 76–85.

Meng, Z., Zhang, Y., Zhang, Q., Chen, X., Liu, L., Komarneni, S., Lv, F., 2017. Novel synthesis of layered double hydroxides (LDHs) from zinc hydroxide. Appl. Surf. Sci. 396, 799–803.

Miyazaki, A., Numata, M., Etou, M., Yonezu, K., Balint, I., Yokoyama, T., 2013. Evidence for tetrahedral AlO_4 formation induced by Zn^{2+} adsorption onto $Al(OH)_3$ gel. Colloids Surf. A 420, 115–121.

Nachtegaal, M., Marcus, M.A., Sonke, J.E., Vangronsveld, J., Livi, K.J.T., van Der Lelie, D., Sparks, D.L., 2005. Effects of in situ remediation on the speciation and bioavailability of zinc in a smelter contaminated soil. Geochim. Cosmochim. Acta 69, 4649–4664.

Pakalns, P., 1965. Spectrophotometric determination of aluminium with chrome azurol S. Anal. Chim. Acta 32, 57–63.

Piccinno, F., Gottschalk, F., Seeger, S., Nowack, B., 2012. Industrial production quantities and uses of ten engineered nanomaterials in Europe and the world. J. Nanopart. Res. 14 (1109).

Pushparaj, S.S.C., Forano, C., Prevot, V., Lipton, A.S., Rees, G.J., Hanna, J.V., Nielsen, U.G., 2015. How the method of synthesis governs the local and global structure of zinc aluminum layered double hydroxides. J. Phys. Chem. C 119, 27695–27707.

Pushparaj, S.S.C., Jensen, N.D., Forano, C., Rees, G.J., Prevot, V., Hanna, J.V., Ravnsbæk, D.B., Bjerring, M., Nielsen, U.G., 2016. Structural investigation of Zn(II) insertion in bayerite, an aluminum hydroxide. Inorg. Chem. 55, 9306–9315.

Ravel, B., Newville, M., 2005. ATHENA, ARTEMIS, HEPHAESTUS: data analysis for X-ray absorption spectroscopy using IFEFFIT. J. Synchrotron Radiat. 12, 537–541.

Saniger, J., 1995. Al-O infrared vibrational frequencies of γ-alumina. Mater. Lett. 22, 109–113.

Siebecker, M., Li, W., Khalid, S., Sparks, D., 2014. Real-time QEXAFS spectroscopy measures rapid precipitate formation at the mineral–water interface. Nat. Commun. 5 (5003).

Stark, W.J., 2011. Nanoparticles in biological systems. Angew. Chem. Int. Ed. 50, 1242–1258.

Sun, P., Shijirbaatar, A., Fang, J., Owens, G., Lin, D., Zhang, K., 2015. Distinguishable transport behavior of zinc oxide nanoparticles in silica sand and soil columns. Sci. Total Environ. 505, 189–198.

Tarte, P., 1967. Infra-red spectra of inorganic aluminates and characteristic vibrational frequencies of AlO_4 tetrahedra and AlO_6 octahedra. Spectrochim. Acta A 23, 2127–2143.

Tong, T., Fang, K., Thomas, S.A., Kelly, J.J., Gray, K.A., Gaillard, J.-F., 2014. Chemical interactions between nano-ZnO and nano-TiO_2 in a natural aqueous medium. Environ. Sci. Technol. 48, 7924–7932.

Tong, T., Wilke, C.M., Wu, J., Binh, C.T.T., Kelly, J.J., Gaillard, J.-F., Gray, K.A., 2015. Combined toxicity of nano-ZnO and nano-TiO_2: from single- to multinanomaterial systems. Environ. Sci. Technol. 49, 8113–8123.

Tóth, I.V., Rangel, A.O.S.S., Santos, J.L.M., Lima, J.L.F.C., 2004. Determination of aluminum (III) in crystallized fruit samples using a multicommutated flow system. J. Agric. Food Chem. 52, 2450–2454.

Trainor, T.P., Brown, G.E., Parks, G.A., 2000. Adsorption and precipitation of aqueous Zn(II) on alumina powders. J. Colloid Interface Sci. 231, 359–372.

Uekawa, N., Yamashita, R., Jun Wu, Y., Kakegawa, K., 2004. Effect of alkali metal hydroxide on formation processes of zinc oxide crystallites from aqueous solutions containing $Zn(OH)_4^{2-}$ ions. Phys. Chem. Chem. Phys. 6, 442–446.

Voegelin, A., Kretzschmar, R., 2005. Formation and dissolution of single and mixed Zn and Ni precipitates in soil: evidence from column experiments and extended X-ray absorption fine structure spectroscopy. Environ. Sci. Technol. 39, 5311–5318.

Voegelin, A., Scheinost, A.C., Bühlmann, K., Barmettler, K., Kretzschmar, R., 2002. Slow formation and dissolution of Zn precipitates in soil: a combined column-transport and XAFS study. Environ. Sci. Technol. 36, 3749–3754.

Voegelin, A., Pfister, S., Scheinost, A.C., Marcus, M.A., Kretzschmar, R., 2005. Changes in zinc speciation in field soil after contamination with zinc oxide. Environ. Sci. Technol. 39, 6616–6623.

Voegelin, A., Jacquat, O., Pfister, S., Barmettler, K., Scheinost, A.C., Kretzschmar, R., 2011. Time-dependent changes of zinc speciation in four soils contaminated with zincite or sphalerite. Environ. Sci. Technol. 45, 255–261.

Wang, H., Adeleye, A.S., Huang, Y., Li, F., Keller, A.A., 2015. Heteroaggregation of nanoparticles with biocolloids and geocolloids. Adv. Colloid Interf. Sci. 226, 24–36.

Xu, Z.P., Lu, G.Q., 2005. Hydrothermal synthesis of layered double hydroxides (LDHs) from mixed MgO and Al_2O_3: LDH formation mechanism. Chem. Mater. 17, 1055–1062.

Yan, Y., Li, W., Yang, J., Zheng, A., Liu, F., Feng, X., Sparks, D.L., 2014. Mechanism of myo-inositol hexakisphosphate sorption on amorphous aluminum hydroxide: spectroscopic evidence for rapid surface precipitation. Environ. Sci. Technol. 48, 6735–6742.

Yan, Y., Koopal, L.K., Li, W., Zheng, A., Yang, J., Liu, F., Feng, X., 2015. Size-dependent sorption of *myo*-inositol hexakisphosphate and orthophosphate on nano-gamma-Al_2O_3. J. Colloid Interface Sci. 451, 85–92.

Yan, Y., Wan, B., Jaisi, D.P., Yin, H., Hu, Z., Wang, X., Chen, C., Liu, F., Tan, W., Feng, X., 2018. Effects of myo-inositol hexakisphosphate on Zn (II) sorption on γ-alumina: a mechanistic study. ACS Earth Space Chem. 2018 (2), 787–796.

Zhang, Z.-Z., Cheng, Y.-F., Xu, L.-Z.-J., Bai, Y.-H., Xu, J.-J., Shi, Z.-J., Zhang, Q.-Q., Jin, R.-C., 2018. Transient disturbance of engineered ZnO nanoparticles enhances the resistance and resilience of anammox process in wastewater treatment. Sci. Total Environ. 622–623, 402–409.